Acta Biotheor
DOI 10.1007/s10441-016-9294-z

REGULAR ARTICLE

Basin of Attraction of Solutions with Pattern Formation in Slow–Fast Reaction–Diffusion Systems

B. Ambrosio[1] · **M. A. Aziz-Alaoui**[1]

Received: 5 January 2016 / Accepted: 11 October 2016
© Springer Science+Business Media Dordrecht 2016

Abstract This article is devoted to the characterization of the basin of attraction of pattern solutions for some slow–fast reaction–diffusion systems with a symmetric property and an underlying oscillatory reaction part. We characterize some subsets of initial conditions that prevent the dynamical system to evolve asymptotically toward solutions which are homogeneous in space. We also perform numerical simulations that illustrate theoretical results and give rise to symmetric and non-symmetric pattern solutions. We obtain these last solutions by choosing particular random initial conditions.

Keywords Reaction diffusion systems · Slow–fast analysis · Limit-cycles · Pattern formation · FitzHugh–Nagumo

1 Introduction

Pattern formation arises naturally in widely applications such as chemistry, fluid mechanics, bacteria development, morphogenesis, animals coats designs, visual hallucinations. Among the mathematical models that allow pattern formation, reaction–diffusion (RD) models are quite relevant. Recall that RD systems are partial differential equations with the following form:

$$U_t = F(U) + K\Delta U.$$

Let us recall some striking biological examples of pattern formation whose behavior has been successfully modeled by RD systems. The most famous chemical example is certainly the Belousov–Zhabotinsky family of chemical reactions. A mix of a

✉ B. Ambrosio
benjamin.ambrosio@univ-lehavre.fr

[1] UNIHAVRE, LMAH, FR-CNRS-3335, ISCN, Normandie Univ, 76600 Le Havre, France

Published online: 21 October 2016

solution of sodium bromate and sulfuric acid and a solution of malonic acid sodium bromure, with a few drops of ferroin, in adequate proportions, will oscillate between red and blue color. If the same kind of mixture lies on a petri dish, one can observe target or spiral pattern formation. Other patterns such as Turing structures or standing waves have also been observed in Belousov–Zhabotinsky chemical reaction types, see Epstein and Showalter (1996), Mikhailov and Showalter (2006), Taylor (2002), Winfree (2006), Zhabotinsky (2007). Bacteria development also furnishes striking examples of patterns. In this context, RD systems have been successfully used to obtain diffusion-limited aggregation-like, Eden-like, concentric ring-like, disk-like and dense branching morphology-like patterns for the bacteria Bacillus Subtilis development, see Lacasta et al. (1999), Matsushita et al. (1998), Mimura et al. (2000). Dictyostellium Discodeum amoeba, in condition of starvation also exhibits spectacular patterns that have been modelled by RD systems, see Halloy et al. (1998), Lauzeral et al. (1997). In physiological context, spiral or target patterns can be found in excitable or oscillatory cells such as cardiac tissue or brain, see Murray (2010). A well known example of pattern formation in this area is the appearance of visual patterns related to drug induced hallucinations. A mathematical modeling approach has been developed for that, see Ermentrout and Cowan (1979), Golubitsky et al. (2004) and references therein cited. The first mathematical well-known analysis came with the seminal work of Turing (1952), in which a two-component RD system is proposed to explain the morphogenesis. Mathematically, the phenomenon known as Turing mechanism occurs when the diffusion-less system possesses a stable stationary solution and the diffusion term turns the stationary point unstable, leading to stable pattern solutions. The mathematical technique, largely used, consists then on exhibiting sufficient conditions in order to obtain positive eigenvalues for the Jacobian at the steady state, see for example Murray (2010). Analogously, one can obtain stable patterns if the underlying ODE system possesses a bistability property. When the underlying ODE is either excitable or oscillatory, wave propagation may occur that eventually results on pattern formation. In the context of excitable media, wave propagation results from the diffusion term: the excitation wave may propagate trough excitation of neighbors. Notice that this idea already appears in the early works of Rashevsky, see (Rashevsky 1933a, b, 1937). In the case of oscillatory media the wave propagation results from a shift in oscillations regarding to the space location. Note that symmetry plays a key role in pattern formation. This idea was already found in Turing (1952). Since this pioneering work, an important and interesting theory has been developed to study the role of symmetry in dynamical systems, see Golubitsky and Stewart (2002). Among all these cases where RD systems may lead to pattern formation, we focus on the following one: RD systems with two equations and a symmetric oscillatory reaction term. We focus on the characterization of the basin of attraction of special patterns for reaction–diffusion systems whose underlying ODE reaction system has the following property: the unique fixed point is the origin and any solution starting at a value distinct from the origin evolves asymptotically around a unique limit cycle. We will also assume that, the ODE has a symmetry property, for example if $U(t)$ is a solution, $-U(t)$ also is a solution. Such a typical ODE system is given by the following *FitzHugh–Nagumo* equations:

$$\begin{cases} \epsilon u_t = f(u) - v \\ v_t = u - \delta v \end{cases} \tag{1}$$

where $f(u) = -u^3 + 3u$, ϵ is small parameter, and δ not to large in order to ensure the existence of a unique fixed point. Let us recall that the FitzHugh–Nagumo system is a simplification of the Hodgkin–Huxley model which can exhibit oscillatory or excitable behavior. In this system, the variable u represents the cellular electric potential while the variable v is a recovery variable, see Ambrosio and Aziz-Alaoui (2012), FitzHugh (1961), Françoise (2005), Hodgkin and Huxley (1952), Nagumo et al. (1962). In the case studied here, it is oscillatory. This is a slow–fast system. The slow manifold is given by the equation $v = f(u)$. There are two attractive parts in this manifold which correspond to $|u| > 1$. The Fig. 1 illustrates the asymptotic dynamics of system (1).

Throughout this paper, we deal with the following RD system:

$$\begin{cases} \epsilon u_t = f(u) - v + d_u \Delta u \\ v_t = u - \delta v + d_v \Delta v \end{cases} \tag{2}$$

with $f(u) = -u^3 + 3u$, ϵ small, δ not to large, $d_u > 0, d_v \geq 0$ and Neumann Boundary conditions (NBC), even though theoretical results remain valid for systems with analog properties. We are interested in the characterization of the basin of attraction of (2). More precisely, we know that the system generates a semi-group and possesses a global attractor in $L^2(\Omega) \times L^2(\Omega)$ and a bound in $L^\infty(\Omega) \times L^\infty(\Omega)$, see for example Ambrosio et al. (2015), Ambrosio and Françoise (2009), Marion (1989). Note that other frameworks are possible such as classical and Holder function spaces, see Rothe (1984). Among the solutions lying in the attractor, some

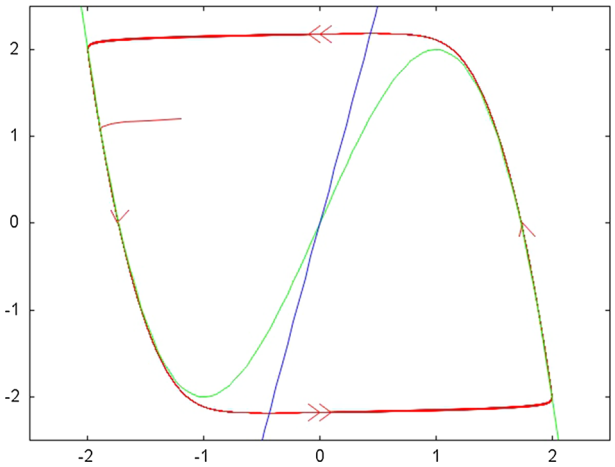

Fig. 1 Asypmtotic behavior of solutions of system (1). Any solution starting at a point distinct from the origin evolves asymptotically toward a unique limit-cycle. In *red* we represent a solution. In *green*, we represent the cubic null-cline corresponding to the first equation while in *blue* we represent the linear null-cline corresponding to the second equation. Note that, due to the ϵ, there is two time scales. The solution reaches rapidly a region near the slow manifold, and then evolve slowly therein. (Color figure online)

are well-known: those constant in space and belonging to the attractor of (1). If we choose initial conditions of (2), $(u_0(x), v_0(x))$ constant in space, and if (u, v) is a solution of (2), then for all fixed $x \in \Omega$, $[u(x, t), v(x, t)]$ is a solution of (1) which evolve asymptotically toward the limit-cycle as soon as $[u_0(x), v_0(x)] \neq (0, 0)$. Numerical simulations show that most of initial conditions evolve asymptotically toward this solution. In the case where,

$$\lambda d_u > 3, \tag{3}$$

where λ is the smallest non-zero eigenvalue of $-\Delta$ with *NBC*, all the solutions evolve asymptotically towards space homogeneous solutions, that is, toward the limit cycle of (1) or toward (0, 0), see Ambrosio and Aziz-Alaoui (2012, 2013), Conway et al. (1978).

A question naturally arises: when (3) is not fulfilled, are we able to characterize the initial conditions that will not evolve toward homogeneous space solutions?

The aim of this article is to discuss this question and furnish some theoretical and numerical elements of response. Indeed, the article is divided in four sections as follows. After the present introduction, we enunciate in the second section, two propositions that give insights on the characterization of the slow-manifold for (2) written around the limit-cycle of (1), and the behavior within this manifold. In the third section, we state sufficient conditions ensuring an asymptotic non-homogeneous space behavior [or maybe evolution toward (0, 0)]. Thus we characterize elements of the basin of attraction of functions of the the attractor distinct from the limit-cycle of (1). For this we use the symmetry of the Eq. (2): if (u, v) is a solution, also $-(u, v)$ is. Besides, we consider symmetric domains. Indeed, we are able to choose appropriate initial conditions, leading to null integrals $\int_\Omega u dx$ and $\int_\Omega v dx$. Therefore, this prevents the solution to evolve toward the limit cycle of (1). In the fourth section, we perform numerical simulations. We illustrate some applications of the theoretical results of the third part and also exhibit numerically other initial conditions that evolve asymptotically to non-homogeneous space solutions (Figs. 2–12). To this aim, we choose initial conditions distributed along stochastic laws with null expectancy and show numerical evidence that this lead to asymptotically non-homogeneous space solutions with no apparent symmetry (Figs. 9–12).

Throughout the paper, we denote by $(\tilde{u}, \tilde{v})$ the periodic solution of (1).

2 The Slow Manifold of (2) Written Around $(\tilde{\mathbf{u}}, \tilde{\mathbf{v}})$

In this section we give two propositions giving insights on the existence of the manifold, when we write (2) around $(\tilde{u}, \tilde{v})$, and on the behaviour within this manifold. System (2) around $(\tilde{u}, \tilde{v})$ reads as:

$$\begin{cases} \epsilon u_t = f'(\tilde{u})u + \dfrac{f''(\tilde{u})}{2}u^2 - u^3 - v + d_u \Delta u \\ v_t = u - \delta v + d_v \Delta v \end{cases} \tag{4}$$

A classical approach to study ODE's with an ϵ in front of some derivatives, is the geometrical singular perturbation theory (GSPT). By a change of time coordinate

$t = \epsilon\tau$, we obtain an equivalent system. The main idea of the GSPT is to set $\epsilon = 0$ in the two equivalent systems and to study the two resulting systems: the layer system and the reduced system, see for example Desroches et al. (2012), Krupa et al. (2014), Kuehn (2015) and references there in cited for a review.

This is what we do know but for the RD system (4). The layer system reads as,

$$\begin{cases} u_t = f'(\tilde{u}(0))u + \dfrac{f''(\tilde{u}(0))}{2}u^2 - u^3 - v + d_u\Delta u \\ v_t = 0 \end{cases} \tag{5}$$

while the reduced system reads as,

$$\begin{cases} 0 = f'(\tilde{u}(t))u + \dfrac{f''(\tilde{u}(t))}{2}u^2 - u^3 - v + d_u\Delta u \\ v_t = u - \delta v + d_v\Delta v \end{cases} \tag{6}$$

We start with the first proposition which states the existence and the local uniqueness of a slow attractive manifold. In our case this leads to an elliptic equation. Let us consider the general equation:

$$u_t = g(u) - v + d_u\Delta u. \tag{7}$$

We have:

Proposition 1 *Let $X = C^0(\bar{\Omega})$endowed with the norm $||f|| = \sup_{x\in\bar{\Omega}}|f(x)|$. We assume that $g \in C^1(\mathbb{R})$is such that $g(0) = 0$ and $g'(0) < 0$, then for $||v||$ small enough and $u_0 \in X \cap C^2(\bar{\Omega})$ such that $||u_0||$ small enough the solution u of (7) evolves towards the (locally) unique stationary solution of (7) in X.*

Proof The proof basically relies on maximum principles, see Protter and Weinberger (1984). We give here a direct proof. Since $g'(0) < 0$, g is locally decreasing in a closed interval I containing 0, for $||v||$ small enough, we can find u_0 and two constant values a and $b \in I$ such that $a < u_0(x) < b$, with:

$$g(b) < v(x) < g(a)$$

and $g'(x) < 0$ in $[a, b]$. This means that a is sub-solution and b an upper-solution of (7), see for example Smoller (1994). Let us denote by $u_a(x, t)$ the solution of (7) with $u_a(x, 0) = a$, then for all $t > 0$, $a < u_a < b$. Indeed, if u_a reaches b for the first time, Eq. (7) leads to $0 \leq \frac{\partial}{\partial t}u_a = g(b) - v + d_u\Delta u_a < 0$, which is not possible. Analogously, since $\frac{\partial}{\partial t}u_a(x, 0) = g(a) - v > 0$, u_a is greater than a for t small enough. Therefore, if u_a reaches a for the first time, we have $0 \geq \frac{\partial}{\partial t}u_a = g(a) - v + d_u\Delta u_a > 0$ which is not possible. Therefore, for all $t > 0$, $a < u_a < b$. Note that this result remains valid for any solution satisfying $a \leq u_0 \leq b$, however we focus for the moment on the solution with $u_0 = a$. We set $w = \frac{\partial}{\partial t}u_a$. Then

$$w_t = g'(u_a)w + d_u\Delta w, \tag{8}$$

and

$$w_0 = g(a) - v > 0.$$

By analog arguments we can prove that $w \geq 0$ (consider the first time for which w reaches a negative value). We prove that in fact, $w > 0$ and we give an uniform bound, depending only on time. Let $l_m = \min_{x\in[a,b]} g'(x)$ and $l_M = \max_{x\in[a,b]} g'(x)$. We have $l_m < l_M < 0$. Let $\underline{w}$ the solution of $w_t = l_m w$ with $\underline{w}_0 = \inf_{x\in[a,b]} w_0$. Then we have

$$w_t \geq l_m w + d_u \Delta w,$$

and therefore,

$$(w - \underline{w})_t \geq l_m(w - \underline{w}) + d_u \Delta(w - \underline{w}).$$

Hence $w - \underline{w} \geq 0$, which means:

$$\frac{\partial}{\partial t} u_a \geq \underline{w}_0 e^{l_m t}.$$

Using the same arguments, we show that $\frac{\partial}{\partial t} u_a = w$ converges uniformly toward 0. Let u_b the solution of (7) with $u(0) = b$, u_b converges uniformly to a continuous function. By analog comparison arguments we show that $u_b - u_a$ converges uniformly toward 0. Indeed, let $h = u_b - u_a$, we have,

$$h_t = g'(\theta)h + d_u \Delta h$$

with $\theta(x,t) \in]a,b[$. We have $h \geq 0$. Let $\bar{h}$ solution of $h_t = l_M h$ with $\bar{h}_0 = \max_{x\in\bar{\Omega}}(u_b - u_a)$ and $\underline{h}$ solution of $h_t = l_m h$ with $\underline{h}_0 = \min_{x\in\bar{\Omega}}(u_b - u_a)$. Then,

$$h_t \leq l_M h + d_u \Delta h,$$

and

$$(\bar{h} - h_t) \leq l_M(\bar{h} - h) + d_u \Delta(\bar{h} - h).$$

Also,

$$(h - \underline{h})_t \geq l_m(h - \underline{h}) + d_u \Delta(h - \underline{h}).$$

Therefore,

$$\underline{h}_0 e^{l_m t} \leq h \leq \bar{h}_0 e^{l_M t}.$$

It follows that h converges uniformly toward 0. Therefore, u_a and u_b converge uniformly toward a function, let's say u^*. Now, we show that u^* is a solution of $g(b) - v + d_u \Delta u = 0$. As $\frac{\partial}{\partial t} u_a$ converges uniformly toward 0, we have

$$g(u^*) - v + d_u \Delta u^* = 0. \tag{9}$$

Also, as $\frac{\partial}{\partial t} u_a$ and $g(u_a)$ converge uniformly, this implies that Δu_a converges uniformly. The same arguments are valid to show that any solution of (7), starting with

$u_0 \in [a, b]$, converges uniformly toward a solution of (9). For the uniqueness, let u_1 and u_2 two solutions of the stationary equation belonging to the interval $[a, b]$. Then:

$$g'(\theta)(u_1 - u_2) + d_u\Delta(u_1 - u_2) = 0.$$

Integrating by parts (or by a maximum principle) leads to $u_1 - u_2 = 0$. □

The proposition 2 gives the qualitative behavior on the attractive part of the slow manifold. More precisely, let $g(t,u) = f'(\tilde{u}(t))u + \frac{f''(\tilde{u}(t))}{2}u^2 - u^3 = 3(1-\tilde{u}^2)u - 3\tilde{u}u^2 - u^3$. The sufficient assumption in the proposition is that $g(t,u)u \leq 0$ which is verified as long as $(\tilde{u}, \tilde{v})$ and (u, v) remain in the attractive parts of the cubic. Then the proposition states that the reduced system decreases exponentially in norm L^2. Let $v(x, t)$ a solution of (6).

Proposition 2 *Let $I = [t_0, t_1]$ such for all $t \in I, g(t,u)u \leq 0$. Then for all $t \in [t_0, t_1]$, we have*

$$\int_\Omega v^2(x,t)dx \leq e^{-\delta(t-t_0)} \int_\Omega v^2(x,0)dx$$

Proof We multiply the second Eq. (6) by v and integrate over Ω, we obtain:

$$\frac{d}{dt}\int_\Omega v^2(x,t)dx = 2\left(\int_\Omega uvdx - \delta\int_\Omega v^2dx + \int_\Omega v\Delta vdx\right).$$

Now, multiplying the first Eq. (6) by u and integrating over Ω, we obtain,

$$\int_\Omega uvdx = \int_\Omega g(t,u)udx + \int_\Omega ud_u\Delta udx.$$

Therefore, using green formula, we obtain:

$$\frac{d}{dt}\int_\Omega v^2(x,t)dx \leq -2\delta\int_\Omega v^2dx.$$

Multiplying by $e^{2\delta t}$ and integrating, we obtain the result. □

3 A Condition for Evolution Toward Patterns

The following theorem exhibits initial conditions that prevent the solution of (2) to evolve toward $(\tilde{u}, \tilde{v})$.

Theorem 1 *Assume that we can divide the domain into a partition $\Omega = (\cup_{i\in\{1,\ldots,l\}} U_i) \cup (\cup_{i\in\{1,\ldots,l\}} V_i)$ such that for $i \in \{1, \ldots, l\}$ there exists a diffeomorphism ϕ_i from U_i to V_i with $|\det J_{\phi_i}| = 1$, where J is the jacobian, and initial conditions, such that for all $x \in \cup_{i\in\{1,\ldots,l\}} U_i)$ and for all $t \in \mathbb{R}^+$, $(u(\phi_i(x),t), v(\phi_i(x),t)) = -(u(x,t), v(x,t))$ then the solution of (2) can not evolve asymptotically toward $(\tilde{u}, \tilde{v})$.*

Proof If the hypothesis of Theorem 1 is satisfied then, for all $t > 0$:

$$\begin{aligned}\int_\Omega u(x,t)dx &= \sum_{i=1}^{l}\int_{U_i} u(x,t)dx + \sum_{i=1}^{l}\int_{V_i} u(x,t)dx \\ &= \sum_{i=1}^{l}\int_{U_i} u(x,t)dx + \sum_{i=1}^{l}\int_{U_i} u(\phi_i(x),t)|\det J_{\phi_i}|dx \\ &= \sum_{i=1}^{l}\int_{U_i} u(x,t)dx - \sum_{i=1}^{l}\int_{U_i} u(x,t)dx \\ &= 0.\end{aligned}$$

The result is valid for $\int_\Omega v(x,t)dx$. And we know that for all t:

$$\int_\Omega (\tilde{u}(t), \tilde{v}(t)) \neq (0,0).$$

□

The two following corollaries give examples of situations where Theorem 1 applies.

Corollary 1 *Assume that the domain Ω has (0, 0) for symmetry center and that for all $x = (x_1, x_2) \in \Omega, (u_0, v_0)(x) = -(u_0, v_0)(-x)$ then for all $t > 0$ and for all $x \in \Omega, (u, v)(x, t) = -(u, v)(-x, t)$. Then the solution of (2) cannot evolve asymptotically toward $(\tilde{u}, \tilde{v})$.*

Proof This follows from symmetry, and the property that $(f(-u) + v, -u + \delta v) = -(f(u) - v, u - \delta v)$. □

Corollary 2 *Suppose that the domain Ω has $(x_1, 0)$ as a symmetry axis and that for all $x = (x_1, x_2) \in \Omega, (u_0, v_0)(x_1, x_2) = -(u_0, v_0)(x_1, -x_2)$, then for all $t > 0$ and for all $x \in \Omega, (u, v)(x_1, x_2, t) = -(u, v)(x_1, -x_2, t)$. It follows that the solution of (2) cannot evolve asymptotically toward $(\tilde{u}, \tilde{v})$.*

Proof This follows from analog arguments of symmetry. □

4 Numerical Simulations

In this section we present numerical simulations of (2) leading to pattern formation (Figs. 2–12). We use a $C++$ program with a finite-difference scheme in space and RK4 in time. We choose a time step $dt = 0.01$ on the intervall [0, 200] and a space step $h = 1$ on the square domain $[0, 100] \times [0, 100]$. Also, we choose $d_u = 1, d_v = 0, \epsilon = 0.1, \delta = 0.2$. Numerical simulations are shown in figures above.

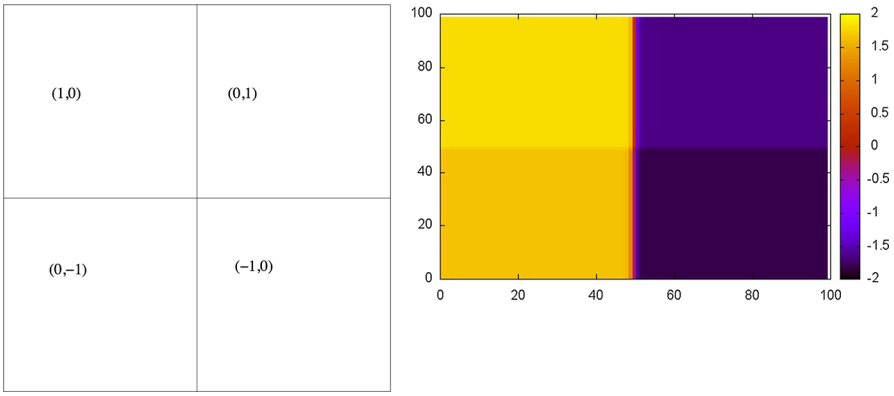

Fig. 2 In the *left panel* we show initial conditions leading to spiral asymptotic behavior for (2). We choose $(u_0(x), v_0(x)) = (1, 0)$ on the *quarter left-up square*, $(u_0(x), v_0(x)) = (0, 1)$ on the *quarter right-up square*, $(u_0(x), v_0(x)) = (0, -1)$ on the *quarter left-down square* and $(u_0(x), v_0(x)) = (-1, 0)$ on the *quarter right-down square*. In the *right panel*, we show the isovalues of $u(x_1, x_2, 0.1)$

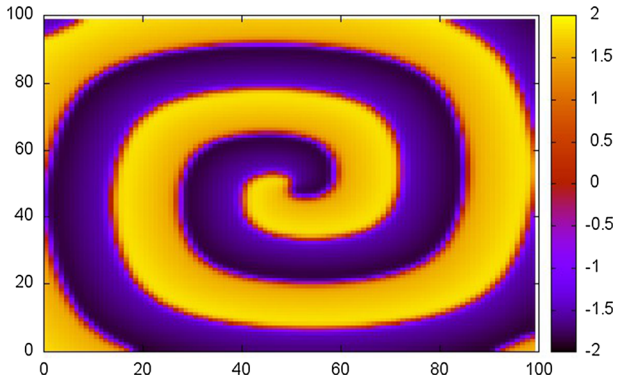

Fig. 3 This figure shows the asymptotical evolution of a solution of (2). More precisely, it represents the isovalues of $u(x_1, x_2, t)$ for time $t = 190$. It is obtained by choosing $(u_0(x), v_0(x)) = (1, 0)$ on the *quarter left-up square*, $(u_0(x), v_0(x)) = (0, 1)$ on the *quarter right-up square*, $(u_0(x), v_0(x)) = (0, -1)$ on the *quarter left-down square* and $(u_0(x), v_0(x)) = (-1, 0)$ on the *quarter right-down square*. See Fig. 2. This illustrates an asymptotic non homogeneous space behavior of a spiral type. It is an application of the Corollary 1

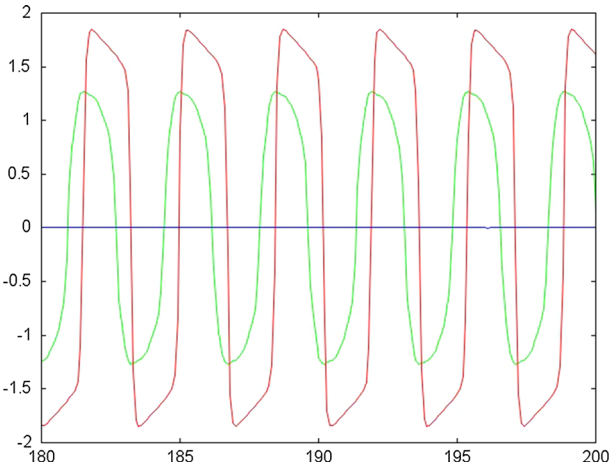

Fig. 4 This figure shows the asymptotic evolution of a solution of (2) at some space points. Indeed, the *green line* represents $u(x_1, x_2, t)$ for $(x_1, x_2) = (50, 50)$, for time $t \in [180, 200]$. The *red line* represents $u(x_1, x_2, t)$ for $(x_1, x_2) = (50, 100)$, for time $t \in [180, 200]$. Finally, the *blue line* represents $\int_\Omega u(x, t)dx$, which is zero as predicted by the theory. It is obtained by choosing the same initial conditions as in Fig. 3. This illustrates an asymptotic non homogeneous space behavior. For each $x \in \Omega$ the trajectory evolves asymptotically around limit cycles of same period, the patterns observed result from a phase shift. (Color figure online)

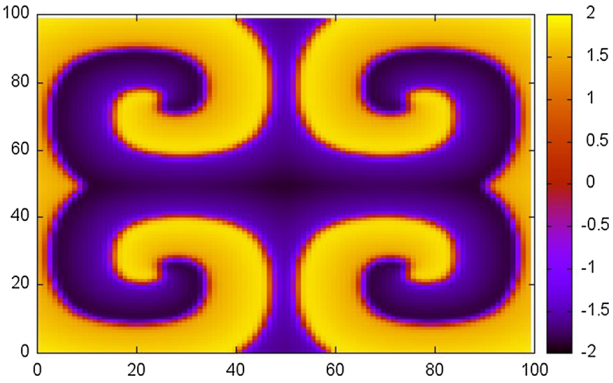

Fig. 5 This figure shows the asymptotic evolution of a solution of (2). It represents $u(x_1, x_2, t)$ for time $t = 190$. It is obtained by reproducing four times the initial conditions of Fig. 3 by axial symmetry. More precisely, we reproduce the initial conditions of Fig. 3 in the *upper-left quarter square*. Then, we operate an axial symmetry of axis $(x_1, 50)$ to obtain the initial conditions on the *quarter down-left square*, and an axial symmetry of axis $(50, x_2)$ to obtain the initial conditions on the *upper-right quarter square*. Finally, we choose initial conditions on the *down-right quarter* by central symmetry of the *upper-left* or equivalently by axial symmetry of the *upper-right* or *down-left quarter square*. Then, we obtain four spirals. By the way, we can show by symmetry that choosing such initial conditions, implies that the solution on the *upper-left* quarter verify (2) with NBC. Then, it comes from symmetry that we obtain four times the same patterns. We can repeat this procedure as many times as needed

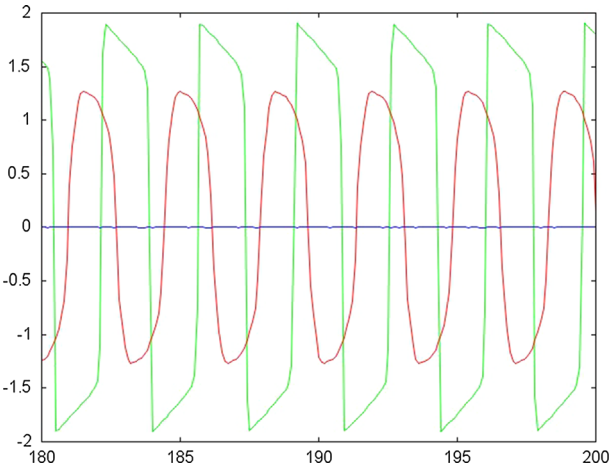

Fig. 6 This figure shows the asymptotic evolution of a solution of (2) at some space points. Indeed, the *green line* represents $u(x_1, x_2, t)$ for $(x_1, x_2) = (50, 50)$, for time $t \in [180, 200]$. The *red line* represents $u(x_1, x_2, t)$ for $(x_1, x_2) = (50, 100)$, for time $t \in [180, 200]$. Finally, the *blue line* represents $\int_\Omega u(x, t)dx$, for time $t \in [180, 200]$, which is zero as predicted by the theory. It is obtained by choosing the same initial conditions as in Fig. 5. This illustrates an asymptotic non homogeneous space behavior. For each $x \in \Omega$ the trajectory evolves asymptotically around limit cycles of same period, the patterns observed result from a phase shift. (Color figure online)

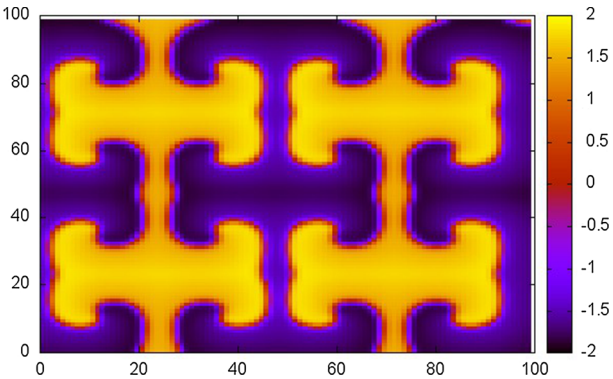

Fig. 7 This figure shows the asymptotic evolution of a solution of (2). It represents $u(x_1, x_2, t)$ for time $t = 190$. It is obtained by operating two times the procedure described in Fig. 5. We obtain sixteen spirals. However, we have to notice that in this case, because of our discretization, we don't have a perfect symmetry for initial conditions. Indeed, some domains are slightly larger than other, for example the left-down corner in which we take a constant initial contain 13×13 (because $13 = \lfloor 100/8 \rfloor + 1$) points while the opposite region where we choose symmetric value contains 12×12 points. Therefore, the symmetry is not perfectly verified

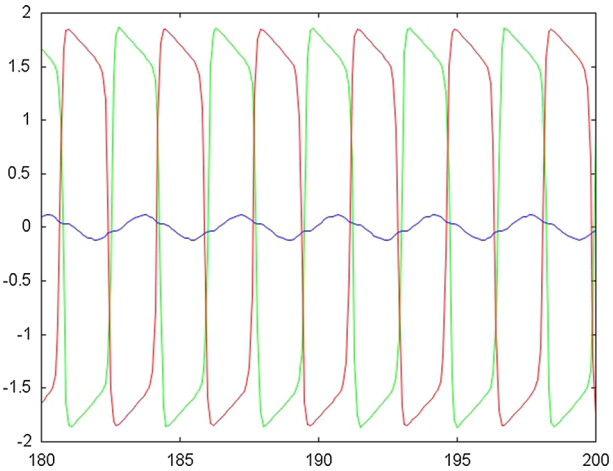

Fig. 8 This figure shows the asymptotic evolution of a solution of (2) at some space points. Indeed, the *green line* represents $u(x_1, x_2, t)$ for $(x_1, x_2) = (50, 50)$, for time $t \in [180, 200]$. The *red line* represents $u(x_1, x_2, t)$ for $(x_1, x_2) = (50, 100)$, for time $t \in [180, 200]$. Finally, the *blue line* represents $\int_\Omega u(x, t)dx$, for time $t \in [180, 200]$. It is obtained by choosing the same initial conditions as in Fig. 7. This illustrates an asymptotic non homogeneous space behavior. For each $x \in \Omega$, the trajectory evolves asymptotically around limit cycles of same period, the patterns observed result from a phase shift. Here the value of $\int_\Omega u(x, t)dx$ is non zero, but rather periodic. Here the theoretical results of the previous section do not apply as our initial solutions do not satisfy the symmetric conditions. (Color figure online)

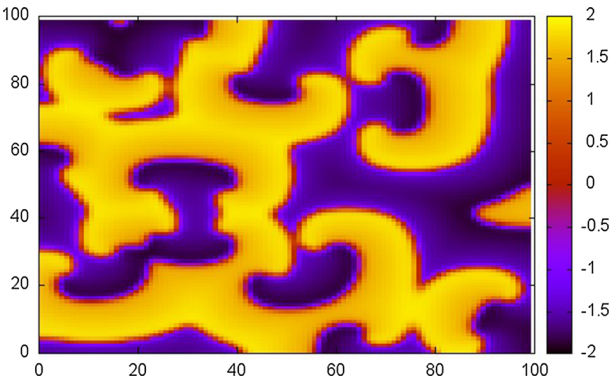

Fig. 9 This figure shows the asymptotic evolution of a solution of (2). More precisely, it represents $u(x_1, x_2, t)$ for time $t = 190$. It is obtained by choosing for all $x \in \Omega$, $(u_0(x), v_0(x))$ as a realization of an uniform stochastic variable on $[-1, 1]$. This illustrates an asymptotic non homogeneous space behavior

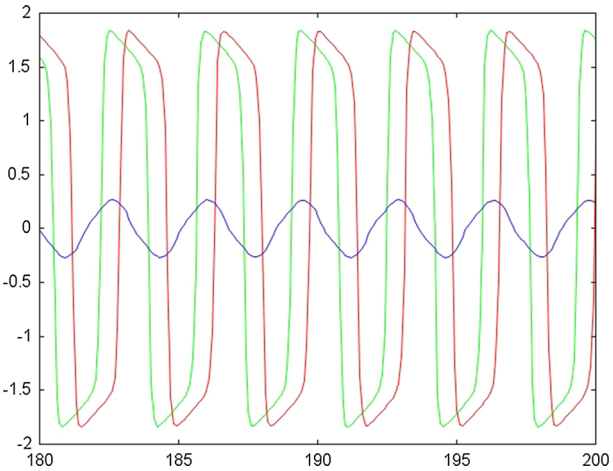

Fig. 10 This figure shows the asymptotic evolution of a solution of (2) at some space points. Indeed, the *green line* represents $u(x_1, x_2, t)$ for $(x_1, x_2) = (50, 50)$, for time $t \in [180, 200]$. The *red line* represents $u(x_1, x_2, t)$ for $(x_1, x_2) = (50, 100)$, for time $t \in [180, 200]$. Finally, the *blue line* represents $\int_\Omega u(x, t)dx$, for time $t \in [180, 200]$. As previously the figure is obtained by choosing for all $x \in \Omega$, $(u_0(x), v_0(x))$ as a realization of an uniform stochastic variable on $[-1, 1]$. This illustrates an asymptotic non homogeneous space behavior. For each $x \in \Omega$ the trajectory evolves asymptotically around the same limit cycle, the patterns observed result from a phase shift. We can see that the value of $\int_\Omega u(x, t)dx$ oscillate between approximatively -0.3 and 0.3 as it was the case for the solution with sixteen spirals. In this case also the zero-integral condition with symmetry is not verified for initial conditions. (Color figure online)

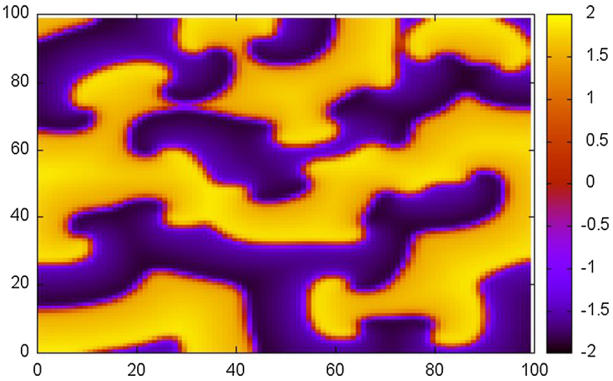

Fig. 11 This figure shows the asymptotic evolution of a solution of (2). More precisely, it represents $u(x_1, x_2, t)$ for time $t = 190$. It is obtained by choosing for all $x \in \Omega$, $(u_0(x), v_0(x))$ as a realization of a stochastic variable following the law $\mathcal{N}(0, 1)$. This illustrates an asymptotic non homogeneous space behavior as it was the case for stochastic uniform initial conditions

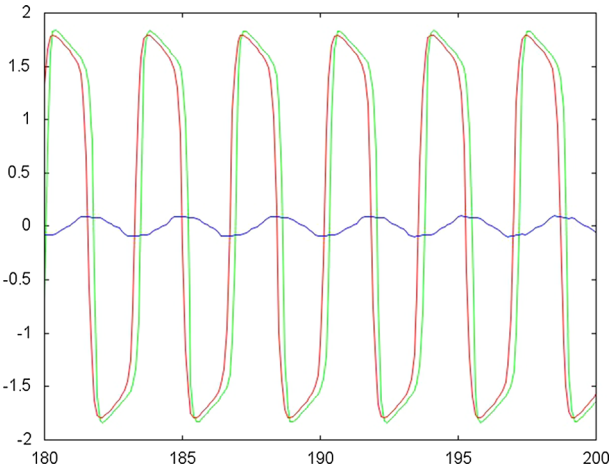

Fig. 12 This figure shows the asymptotic evolution of a solution of (2) at some space points. The *green line* represents $u(x_1, x_2, t)$ for $(x_1, x_2) = (50, 50)$, for time $t \in [180, 200]$. The *red line* represents $u(x_1, x_2, t)$ for $(x_1, x_2) = (50, 100)$, for time $t \in [180, 200]$. Finally, the *blue line* represents $\int_\Omega u(x, t)dx$, for time $t \in [180, 200]$. As previously the figure is obtained by choosing for all $x \in \Omega$, $(u_0(x), v_0(x))$ as a realization of a stochastic variable following the law $\mathcal{N}(0, 1)$. This illustrates an asymptotic non homogeneous space behavior. For each $x \in \Omega$ the trajectory evolves asymptotically around the same limit cycle, the patterns observed result from a phase shift. As previously the value of $\int_\Omega u(x, t)dx$ oscillate between approximately -0.1 and 0.1. (Color figure online)

Acknowledgments Some part of this research has been done during the visiting period of the first author at CIMS, NYU in 2014–2015. He would like to thank L. Mertz, as some interesting discussions during this period, became concrete in this paper. The authors would like to thank Région Haute Normandie and—FEDER (RISC project) for financial support.

References

Ambrosio B, Françoise JP (2009) Propagation of bursting oscillations. Philos Trans R Soc A 367:4863–4875

Ambrosio B, Aziz-Alaoui MA (2012) Synchronization and control of coupled reaction–diffusion systems of the fitzhugh–nagumo type. Comput Math Appl 64:934–943

Ambrosio B, Aziz-Alaoui MA (2013) Synchronization and control of a network of coupled reaction–diffusion systems of generalized fitzhugh-nagumo type. In: ESAIM:Proceedings 39

Ambrosio B, Aziz-Alaoui M, Phan V (2015) Attractor and synchronization for a complex network of reaction–diffusion systems of fitzhugh–nagumo type. arXiv:1504.07763v2

Conway E, Hoff D, Smoller J (1978) Large-time behaviour of solutions of systems of non linear reaction–diffusion equations. SIAM J Appl Math 35:1–16

Desroches M, Guckenheimer J, Krauskopf B, Kuehn C, Osinga HM, Wechselberger M (2012) Mixed-mode oscillations with multiple time scales. SIAM Rev 54(2):211–288

Epstein IR, Showalter K (1996) Nonlinear chemical dynamics: oscillations, patterns, and chaos. J Phys Chem 100:13132–13147

Ermentrout G, Cowan J (1979) A mathematical theory of visual hallucilations patterns. Biol Cybern 34:137150

FitzHugh RA (1961) Impulses and physiological states in theoretical models of nerve membrane. Biophys J 1:445–466

Françoise JP (2005) Oscillations en biologie. Springer

Golubitsky M, Stewart I (2002) The symmetry perspective. Birkhauser

Golubitsky M, Shiau LJ, Torok A (2004) Symmetry and pattern formation on the visual cortex. Dynamics and bifurcation of patterns in dissipative systems. Series on nonlinear. Science 12:3–19
Halloy J, Lauzeral J, Goldbeter A (1998) Modelling oscillations and waves of camp in dictyostelium discoideum cells. Biophys Chem 79:9–19
Hodgkin A, Huxley A (1952) A quantitative description of membrane current and its application to conduction and excitation in nerve. J Physiol 117:500–544
Krupa M, Ambrosio B, Aziz-Alaoui MA (2014) Weakly coupled two slow–two fast systems, folded singularities and mixed mode oscillations. Nonlinearity 27:1555–1574
Kuehn C (2015) Multiple time scale dyanmics. Springer
Lacasta AM, Cantalapiedra IR, Auguet CE, Penaranda A, Ramirez-Piscina L (1999) Modeling of spatiotemporal patterns in bacterial colonies. Phys Rev E 59:7036
Lauzeral J, Halloy J, Goldbeter A (1997) Desynchronization of cells on the developmental path triggers the formation of spiral waves of camp during dictyostelium aggregation. Proc Natl Acad Sci 94:9153–9158
Marion M (1989) Finite-dimensionnal attractors associated with partly dissipative reaction–diffusion systems. SIAM J Math Anal 20:816–844
Matsushita M, Wakita J, Itoh H, Rafols I, Matsuyama T, Sakaguchi H, Mimura M (1998) Interface growth and pattern formation in bacterial colonies. Phys A 249:517–524
Mikhailov A, Showalter K (2006) Control of waves, patterns and turbulence in chemical systems. Phys Rep 425:79–194
Mimura M, Sakaguchi H, Matsushita M (2000) Reaction–diffusion modelling of bacterial colony patterns. Phys A 282:283–303
Murray J (2010) Mathematical biology. Springer
Nagumo J, Arimoto S, Yoshizawa S (1962) An active pulse transmission line simulating nerve axon. Proc IRE 50:2061–2070
Protter MH, Weinberger HF (1984) Maximum principles in differential equations. Springer
Rashevsky N (1933) Outline of a physico-mathematical theory of excitation and inhibition. Protoplasma 20:42–56
Rashevsky N (1933) Some physico-mathematical aspects of nerve conduction. J Appl Phys 4:341–386
Rashevsky N (1937) Mathematical theory of the transmission from of excitation from one tissue to another. Acta Biotheor 3:81–86
Rothe F (1984) Global solutions of reaction–diffusion systems. Springer
Smoller J (1994) Shock waves and reaction diffusion. Springer
Taylor AF (2002) Mechanism and phenomenology of an oscillating chemical reaction. Prog React Kinet Mech 27:247–325
Turing AM (1952) The chemical basis of morphogenesis. Philos Trans R Soc B 237:37–72
Winfree A (2006) Spiral waves of chemical activity. Nature 175:634–636
Zhabotinsky A (2007) Belousov–zhabotinsky reaction. Scholarpedia 2(9):1435